Surrogate Modeling of Time-Dependent Metocean Conditions during Hurricanes

Chi Qiao
Northeastern University
Andrew T. Myers (atm@neu.edu)
Northeastern University

Research Article

Keywords: Time-dependent surrogate modeling, Kriging, Neural Networks, Deep Learning, ocean waves, storm surge

Posted Date: February 23rd, 2021

DOI: https://doi.org/10.21203/rs.3.rs-234266/v1

Surrogate Modeling of Time-Dependent Metocean Conditions during Hurricanes

C. Qiao [a], *A.T. Myers* [a]

[a] *Department of Civil & Environmental Engineering, Northeastern University, Boston, MA, USA*

Abstract

Metocean conditions during hurricanes are defined by multiple parameters (e.g., significant wave height and surge height) that vary in time with significant auto- and cross-correlation. In many cases, the nature of the variation of these characteristics in time is important to design and assess the risk to offshore structures, but a persistent problem is that measurements are sparse and time history simulations using metocean models are computationally onerous. Surrogate modeling is an appealing approach to ease the computational burden of metocean modeling, however, modeling the time-dependency of metocean conditions using surrogate models is challenging because the conditions at one time instant are dependent on not only the conditions at that instant but also on the conditions at previous time instances. In this paper, time-dependent surrogate modeling of significant wave height, peak wave period, peak wave direction, and storm surge is explored using a database of metocean conditions at an offshore site. Three types of surrogate models, including Kriging, Multilayer Perceptron (MLP), and Recurrent Neural Network with Gated Recurrent Unit (RNN-GRU), are evaluated, with two different time-dependent structures considered for the Kriging model and two training set sizes for the MLP model, resulting in a total of five models evaluated in this paper. The performance of the models is compared in terms of accuracy and sensitivity towards hyperparameters, and the MLP and RNN-GRU models are demonstrated to have extraordinary prediction performance in this context.

Keywords: Time-dependent surrogate modeling, Kriging, Neural Networks, Deep Learning, ocean waves, storm surge

1. Introduction

Modeling of metocean conditions (e.g., significant wave height, peak wave period, etc.) during hurricanes is a situation well-suited for surrogate modeling, as the underlying physical processes are complex and numerical models are so computationally demanding that their potential for engineering applications is limited. The term surrogate model refers to a data-driven statistical model that approximates the behavior of a complex process characterized by input (measurable quantities that have relevant predictive power) and output (the variable(s) of interest). Some parametric surrogate models of metocean conditions during hurricanes [1] have been proposed, but these are limited to deep and open waters. However, for more general situations, such as those with limited water depth or fetch length, the conventional practice is to use numerical, time-dependent models [2, 3] that account for important nonlinear phenomena such as wind-sea and wave-wave interactions, energy dissipation, etc. Because the historical record of hurricanes is relatively short, a catalog of synthetic hurricanes representing a much longer period of time is commonly applied in engineering design and risk assessments. Numerical simulations of metocean conditions for each of the thousands of hurricanes in such a catalog are intractable, and a promising approach is to

instead simulate only a small subset of these hurricanes numerically and then create a surrogate model to replace the time-consuming numerical model for simulating the remaining hurricanes.

Surrogate modeling for time-dependent processes, such as metocean conditions during hurricanes, is a challenging task. In this context, time-dependent processes refer to processes with characteristics that vary in time and are affected not only by the current conditions but also by the conditions at previous instances of time. This kind of behavior is difficult for surrogate models to represent because the correlation between the predictions made for different time instances also needs to be captured by surrogate models. Many types of surrogate models have been explored for modeling metocean conditions, including decision trees [4], response surfaces [5], Kriging [6], and support vector machine (SVM) [7]. When applying these models to a time series, each set of input and output are independent of each other, and so these models cannot explicitly model the time-dependency of metocean processes. Some researchers have proposed approaches to adapt these models for time-dependent processes. For example, Jia et al. [8] used Kriging to model storm surge with a high-dimensional vector designed to preserve time-dependence. In addition to the techniques above, Neural Networks are also used for surrogate modeling of metocean conditions, such as [14-16], where the networks utilized by these researchers have a structure with one hidden layer. In recent years, Neural Networks have evolved alongside the rapid development of Deep Learning, resulting in a new family of techniques that are referred to as Deep Neural Networks, which have network structures with multiple hidden layers and more sophisticated layer operations – from the basic operations of a Multilayer Perceptron, MLP, to the complex operations of a Recurrent Neural Network, RNN. These advances have yielded better performance for many complex tasks such as natural language processing [17] and computer vision [18], but their application in the surrogate modeling of metocean conditions is so far limited (refer to [7] as one example).

Development of a surrogate model of time-dependent metocean conditions involves several loosely coupled choices: the size of the training dataset, the selection of the type of surrogate model (e.g., Kriging, MLP, RNN, etc.), and the design of the time-dependent structure. A model with a time-dependent structure has capabilities that can predict a series of output that preserves correlation in time. Some models, like RNN, have inherent time-dependent structures, while others, like Kriging and MLP, do not have such structures inherently. For the latter type of models, the effect of time-dependent processes can be modeled with *ad hoc* manipulation of the input and/or output vectors of the models. In this paper, a database of metocean conditions during hurricanes for an offshore site is used to compare five combinations of the surrogate model, the time-dependent structure, and the size of the training dataset. This paper has two goals: (1) to illustrate how intrinsic characteristics of the surrogate model along with details of its time-dependent structure and size of training dataset affect the overall performance of the model, and (2) to demonstrate the enormous potential of so-called Deep Neural Networks in surrogate modeling of metocean conditions. For the Neural Networks considered in this paper, the influence of the network structure (i.e., the number of hidden layers and the number of units within each hidden layer) is also explored. This paper is organized as follows. First, the background of the surrogate models utilized in this paper is provided in Section 2. Then, the database of metocean conditions during hurricanes, which is used for model training, is described in Section 3. Details of the implementation of the five models considered in this paper are presented in Section 4. Results are provided and discussed in Section 5, and conclusions are summarized in Section 6.

2. Background

Three types of surrogate models are considered in this paper: Kriging, the Multilayer Perceptron (MLP), and Recurrent Neural Network with Gated Recurrent Unit (RNN-GRU) [19]. The latter two models are categorized as Deep Neural Networks. These three types of models are chosen to represent a relevant range of characteristics. For example, the RNN-GRU model has an inherent time-dependent structure and can naturally model time-dependent processes, while the other two require an *ad hoc* arrangement of the input and output vectors to model such processes. Another important distinction is that Kriging is a memory-based approach (i.e., all training data are memorized to make predictions), while the other two are parametric models (i.e., training data is only used to determine a set of parameters of the model and is not directly involved in making predictions). Key features of these models are provided in Table 1, and the details of each model are presented separately in the remainder of this section.

Table 1. Summary of the three surrogate models used in this paper to model time-dependent processes. A list of choices for the key hyperparameters explored in this paper is provided in square brackets.

Surrogate Model	Time-dependent structure?	Memory-based?	Key hyperparameters
Kriging	No	Yes	• Type of regression function: linear • Type of correlation function: exponential
MLP	No	No	• Number of hidden layers: [1, 3, 5, 7] • Number of units per layer: [16, 32, 64, 128, 256, 512, 1024, 2048, 4096] • Activation function: ReLU
RNN-GRU	Yes	No	• Number of hidden layers: [1, 3, 5, 7] • Number of units per layer: [16, 32, 64, 128, 256, 512, 1024, 2048, 4096] • Activation function: hyperbolic tangent • Recurrent activation function: hard sigmoid

2.1 Kriging model

For a training dataset $\left(\boldsymbol{X}_{m\times n}, \boldsymbol{Y}_{m\times q}\right)$ composed of m samples of n input variables and q output variables, the Kriging model uses a linear combination of training output $\boldsymbol{Y}$ to provide the prediction $\hat{\boldsymbol{y}}$ for any unknown input $\tilde{\boldsymbol{x}}$ as,

$$\hat{\boldsymbol{y}} = \boldsymbol{c}^{\top}\boldsymbol{Y} = \boldsymbol{f}(\tilde{\boldsymbol{x}})^{\top}\boldsymbol{\beta}^{*} + \boldsymbol{r}(\tilde{\boldsymbol{x}})^{\top}\boldsymbol{\gamma}^{*} \tag{1}$$

where $\boldsymbol{c}^{\top}$ is the coefficient matrix of the linear combination, $\boldsymbol{f}_{p\times 1}(\boldsymbol{x})$ is the regression function, $\boldsymbol{\beta}^{*}_{p\times q}$ is the result of the generalized least squares method $\boldsymbol{\beta}^{*} = (\boldsymbol{F}^{\top}\boldsymbol{R}^{-1}\boldsymbol{F})^{-1}\boldsymbol{F}^{\top}\boldsymbol{R}^{-1}\boldsymbol{Y}$, $\boldsymbol{F}_{m\times p}$ is the result of the regression function evaluated at all the training inputs $\boldsymbol{F}_{m\times p} = [\boldsymbol{f}(\boldsymbol{x}_1) \dots \boldsymbol{f}(\boldsymbol{x}_m)]^{\top}$, $\boldsymbol{R}_{m\times m}$ is the result of the correlation function $\mathcal{R}\left(\boldsymbol{\theta}, \boldsymbol{x}_i, \boldsymbol{x}_j\right)$ evaluated at all of the training inputs (i.e., $i, j = 1, \dots, m$), $\boldsymbol{r}(\tilde{\boldsymbol{x}})_{m\times 1}$ is the result of the correlation function evaluated between the training inputs and $\tilde{\boldsymbol{x}}$, and $\boldsymbol{\gamma}^{*}_{m\times q}$ is the result of $\boldsymbol{\gamma}^{*} = \boldsymbol{R}^{-1}(\boldsymbol{Y} - \boldsymbol{F}\boldsymbol{\beta}^{*})$. The parameter $\boldsymbol{\theta}$ is optimized to minimize the mean squared error $E[(\hat{\boldsymbol{y}} - \boldsymbol{y})^2]$ of the training dataset.

There are two hyperparameters in the Kriging model, the regression function $f(\boldsymbol{x})$ and the correlation function $\mathcal{R}(\boldsymbol{\theta}, \boldsymbol{x}_i, \boldsymbol{x}_j)$. Possible forms for the function $f(\boldsymbol{x})$ include a constant function $f^{(0)}(\boldsymbol{x}) = 1$, a linear function $f^{(1)}(\boldsymbol{x}) = [1, x_1, \dots, x_n]^\top$, and a quadratic function $f^{(2)}(\boldsymbol{x}) = [1, x_1, \dots, x_n, x_1^2, x_1x_2, \dots, x_n^2]$. In this paper, the linear regression function and the exponential correlation function are used. The constant regression function and two other types of correlation functions, linear and Gaussian (detailed expressions for these are provided in [20]), were included in preliminary experiments, but were found to have higher prediction errors and are not discussed here. Quadratic or higher-order regression functions are not considered because the dimension of $f(\boldsymbol{x})$ exceeds the number of training samples for some cases considered in this paper. Note that the inclusion of some quadratic terms might improve the performance of the regression term $\boldsymbol{f}(\tilde{\boldsymbol{x}})^\top \boldsymbol{\beta}^*$, however, such implementation requires domain knowledge and is not common practice.

2.2 MLP

An MLP model is the most basic Neural Network. It includes several layers of units, with the first layer representing the input vector and the last layer representing the output vector. Figure 1 shows the structure of an MLP model with two hidden layers as an example. The operation of each hidden layer is expressed as,

$$\boldsymbol{z}_2 = g(\boldsymbol{z}_1 \cdot \boldsymbol{W} + \boldsymbol{b}) \tag{2}$$

where, for each layer of the model, $\boldsymbol{z}_1$ is the input vector, $\boldsymbol{z}_2$ is the output vector, $\boldsymbol{W}$ is the weight matrix, $\boldsymbol{b}$ is the vector representing bias, and g is the so-called activation function, which nonlinearly transforms the data elementwise.

Compared to the Kriging model, the MLP model has more hyperparameters. First, the MLP model includes l hidden layers (the number of hidden layers is referred to herein as the depth of the network) and k units per layer (the number of units per layer is referred to herein as the width of the network), which together determine the structure of the network. The ability of the model to approximate nonlinear behavior and the complexity of the training process increase with the number of hidden layers and the number of units per layer. These parameters affect model performance as does the activation function g.

In this paper, the selected activation function is ReLU (Rectified Linear Unit [21], expressed as $y = \max(0, x)$). Three other types of activation functions, namely ELU (Exponential Linear Unit [23]), sigmoid (i.e., standard logistic), and hyperbolic tangent, were considered during preliminary experiments, but ReLU was found to have the best performance and so the others are not discussed here. The number of hidden layers (l = 1, 3, 5, and 7) and the number of units per layer (k = 16, 32, 64, 128, 256, 512, 1024, 2048, and 4096) are investigated to determine the optimal network structure for this application. Note that the number of units per layer k is assumed to be constant for each hidden layer to simplify the optimization, and, as such, each network structure is identified as $l \times k$.

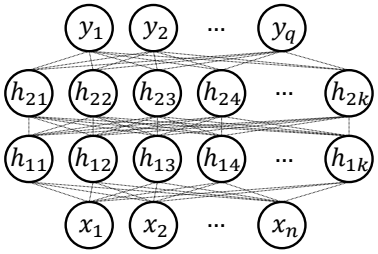

Figure 1. An example MLP model structure with l = 2 hidden layers and k units per hidden layer.

2.3 RNN-GRU

An RNN-GRU model is structured similarly to the MLP model (see Figure 1), but with the output of each layer $\boldsymbol{h}_t$ expressed as,

$$\boldsymbol{u}_t = \sigma(\boldsymbol{x}_t \cdot \boldsymbol{W}_{ux} + \boldsymbol{h}_{t-1} \cdot \boldsymbol{W}_{uh} + \boldsymbol{b}_u) \tag{3}$$

$$\boldsymbol{r}_t = \sigma(\boldsymbol{x}_t \cdot \boldsymbol{W}_{rx} + \boldsymbol{h}_{t-1} \cdot \boldsymbol{W}_{rh} + \boldsymbol{b}_r) \tag{4}$$

$$\widetilde{\boldsymbol{h}}_t = g(\boldsymbol{x}_t \cdot \boldsymbol{W}_{hx} + (\boldsymbol{r}_t * \boldsymbol{h}_{t-1}) \cdot \boldsymbol{W}_{hh} + \boldsymbol{b}_h) \tag{5}$$

$$\boldsymbol{h}_t = (\boldsymbol{1} - \boldsymbol{u}_t) * \boldsymbol{h}_{t-1} + \boldsymbol{u}_t * \widetilde{\boldsymbol{h}}_t \tag{6}$$

where $\boldsymbol{W}_{ux}, \boldsymbol{W}_{uh}, \boldsymbol{W}_{rx}, \boldsymbol{W}_{rh}, \boldsymbol{W}_{hx}, \boldsymbol{W}_{hh}$ are weighting matrices, $\boldsymbol{b}_u, \boldsymbol{b}_r, \boldsymbol{b}_h$ are bias vectors, σ is the recurrent activation function, $*$ indicates elementwise multiplication between two vectors, and t indicates the time instance. For the first time instance $t = 1$, the vector $\boldsymbol{h}_0$ at each layer is initialized as a zero vector and the vector $\boldsymbol{h}_1$ at each layer is calculated according to Eq. 6, which is then used as the vector $\boldsymbol{h}_{t-1}$ to begin predictions at time instance $t = 2$, and so on. The vector $\boldsymbol{u}_t$ in Eq. 6 represents the percent of the past information (i.e., $\boldsymbol{h}_{t-1}$) to be updated, $\boldsymbol{r}_t$ indicates the percent of the past information to forget, and $\widetilde{\boldsymbol{h}}_t$ represents the memory content.

The same 36 network structures are tested for the RNN-GRU model as for the MLP model (i.e., all combinations of four values of l and nine values of k, see Table 1). The activation function g is chosen as hyperbolic tangent, the recurrent activation function σ is chosen as hard sigmoid, following common practice.

3. Database of metocean conditions during hurricanes

The database of metocean conditions used in this paper for training the surrogate models includes conditions during a set of synthetic hurricanes. The synthetic hurricanes are selected from a catalog developed by Liu [25], which uses historical hurricanes to characterize potential hurricane activity in the northeastern part of the Atlantic basin over a span of 100,000 years. The hurricanes are defined using the Holland model [26, 27] in terms of seven parameters: longitude and latitude of the hurricane eye location, the central atmospheric pressure, the radius to maximum wind speed, the translational velocity, the translational direction, and the B parameter. The wind speed and atmospheric pressure fields defined by the Holland model are then used as input to a numerical metocean model Mike 21 (refer to [28] for details). The Mike 21 model couples a hydrodynamic module, which simulates two-dimensional flows based on the depth-integrated, incompressible, Reynolds-averaged Navier-Stokes equations [29], and a spectral wave module, which simulates the growth, propagation, and decay of wind-generated waves and swells based on wave action conservation equations [3], to provide predictions on metocean conditions.

One offshore site near South Carolina is considered in this paper (see Figure 2). The coordinates of this site are (78.87°W, 33.09°N) and the water depth is 17 m. All hurricanes in the catalog that induce a mean wind speed of at least 33 m/s at an elevation of 10 m are simulated, resulting in a total of 5,881 hurricanes over the 100,000-year span of the catalog. Four types of metocean conditions are considered: the significant wave height H_s, the peak wave period T_p, the peak wave direction θ_{H_s}, and the sea surface elevation η (including both tide and storm surge). As such, the database includes information from the 5,881 synthetic hurricanes with various durations and the corresponding hourly values of H_s, T_p, θ_{H_s}, and η.

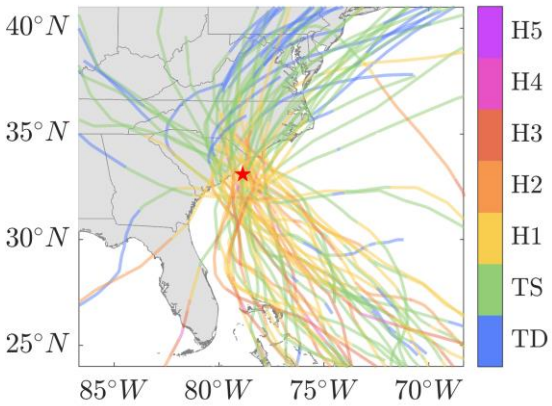

Figure 2. The location of the offshore site near South Carolina (red star) and the trajectories of 50 hurricanes randomly sampled from a total of 5,881 synthetic hurricanes included in the hurricane database. The color of the trajectory indicates the hurricane intensity per the Saffir-Simpson scale (TD stands for tropical depression and TS stands for tropical storm).

4. Numerical experiments

Surrogate modeling is a mathematical mapping between input $\boldsymbol{X}$ and output vectors $\boldsymbol{Y}$, i.e., $\boldsymbol{X} \rightarrow \boldsymbol{Y}$. For the hurricane database introduced in Section 3, $\boldsymbol{Y}$ is a time-dependent vector of four metocean conditions (H_s, T_p, θ_{H_s}, and η) during each hurricane. Five models are introduced in this section, including three types of surrogate models (Kriging, MLP, and RNN-GRU), with two different time-dependent structures considered for the Kriging model and two training set sizes for the MLP model. Some key information for each of the five models is presented in Table 2. The time-dependent structures are introduced in Section 4.1. The design of each of the input vectors $\boldsymbol{X}$ is provided in Section 4.2, and the details of model training and evaluation are provided in Section 4.3.

Table 2. Summary of five models considered in this paper.

	Surrogate model	Time-dependent structure	Number of training samples
Model 1	Kriging	$\boldsymbol{X}(t_{i-k}, \dots, t_i) \rightarrow \boldsymbol{Y}(t_j, \dots, t_{j+l})$	~5,000
Model 2	Kriging	$\boldsymbol{X}(t_{i-k}, \dots, t_i) \rightarrow \boldsymbol{Y}(t_i)$	5,000
Model 3	MLP	$\boldsymbol{X}(t_{i-k}, \dots, t_i) \rightarrow \boldsymbol{Y}(t_i)$	5,000
Model 4	MLP	$\boldsymbol{X}(t_{i-k}, \dots, t_i) \rightarrow \boldsymbol{Y}(t_i)$	~660,000
Model 5	RNN-GRU	$\boldsymbol{X}(t_i) \rightarrow \boldsymbol{Y}(t_i)$	~660,000

4.1 Time-dependent structures

Modeling of metocean conditions during a hurricane can be abstracted as a sequence-to-sequence problem (see Figure 3), where the time-dependent input $\boldsymbol{X}$ represents a set of parameters characterizing the hurricane and site-specific conditions, the time-dependent output $\boldsymbol{Y}$ is the metocean conditions of interest (e.g., H_s, T_p, θ_{H_s}, and η in this paper), and the hidden variables $\boldsymbol{H}$ represent the complex interactions of metocean characteristics. The output at step t_i is affected by not only $\boldsymbol{X}(t_i)$, but also by $\boldsymbol{X}(t_{i-1})$, $\boldsymbol{X}(t_{i-2})$, etc.

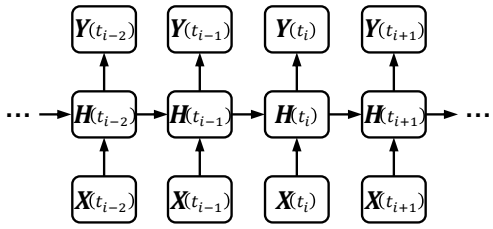

Figure 3. Schematic of the time-dependent structure of a sequence-to-sequence model, where subscripts indicate the time instance, $\boldsymbol{X}$ represents the input vector, $\boldsymbol{H}$ represents a vector of hidden variables, and $\boldsymbol{Y}$ represents the output vector.

For surrogate models without inherent time-dependent structures (e.g., the Kriging and MLP models), the effect of time-dependence can be included with an *ad hoc* arrangement of the input and/or output vectors. Two structures are compared in this paper. The first structure is expressed as $\boldsymbol{X}(t_{i-k}, \dots, t_i) \rightarrow \boldsymbol{Y}(t_j, \dots, t_{j+l})$, a structure that stacks features (the vector $\boldsymbol{X}$ in Figure 3) at steps $t_{i-k}, \dots, t_i$ to form the input vector and predicts an output vector which includes steps $t_j, \dots, t_{j+l}$ (see Figure 4(a)). The vector $\boldsymbol{Y}(t_j, \dots, t_{j+l})$ is selected to cover the time instances corresponding to intense metocean conditions, as these conditions are most important to model accurately for engineering applications. The second structure is expressed as $\boldsymbol{X}(t_{i-k}, \dots, t_i) \rightarrow \boldsymbol{Y}(t_i)$, a structure that predicts metocean conditions independently for each time instance and includes the time-dependence implicitly by stacking input features at various time instances (see Figure 4(b)). At first glance, this structure is a special case of the first structure with $l = 0$. But, there is a philosophical difference between the two structures: the second structure trains and predicts metocean conditions for each hurricane hour, rather than for each hurricane. As such, each hurricane produces multiple training samples, and the duration of predictions is not constant. It is worth noting that the structure $\boldsymbol{X}(t_{i-k}, \dots, t_i) \rightarrow \boldsymbol{Y}(t_j, \dots, t_{j+l})$ can also be implemented in a step-wise manner, i.e., generating multiple training samples for each hurricane, $X(t_{i-k}, \dots, t_i) \rightarrow \boldsymbol{Y}(t_j, \dots, t_{j+l})$, $X(t_{i-k+1}, \dots, t_{i+1}) \rightarrow Y(t_{j+1}, \dots, t_{j+l+1})$, etc. However, this results in multiple predictions for metocean conditions at the same time instance. Thus, the implementation of the first structure in this paper is based on the idea that one hurricane produces one training sample. Also note that, for both structures, the time interval of the input features does not have to match the time interval of the training data. For example, the hurricane database introduced in Section 2 has hourly intervals, but input features can be stacked for time instances with 3-hour intervals. This benefits model performance in some cases, as metocean characteristics with 3-hour intervals are less correlated with each other. Both structures are implemented using the Kriging model (see Model 1 and Model 2 in Table 2), while the second structure is also implemented using the MLP model (see Model 3 and Model 4 in Table 2).

For the RNN-GRU model, the prediction of time-dependent processes is straightforward because it inherently models time-dependent processes. The RNN-GRU model considers input vectors at

each time instance and makes predictions with the following the structure $\boldsymbol{X}(t_i) \rightarrow \boldsymbol{Y}(t_i)$. This structure is considered in Model 5 in Table 2. All three time-dependent structures are summarized in Table 3.

Table 3. Summary of three time-dependent structures considered in this paper.

Time-dependent structure	Requires surrogate models with time-dependent characteristics?	Training samples per hurricane	Model # in Table 2
$\boldsymbol{X}(t_{i-k}, \dots, t_i) \rightarrow \boldsymbol{Y}(t_j, \dots, t_{j+l})$	No	one	1
$\boldsymbol{X}(t_{i-k}, \dots, t_i) \rightarrow \boldsymbol{Y}(t_i)$	No	multiple	2~4
$\boldsymbol{X}(t_i) \rightarrow \boldsymbol{Y}(t_i)$	Yes	multiple	5

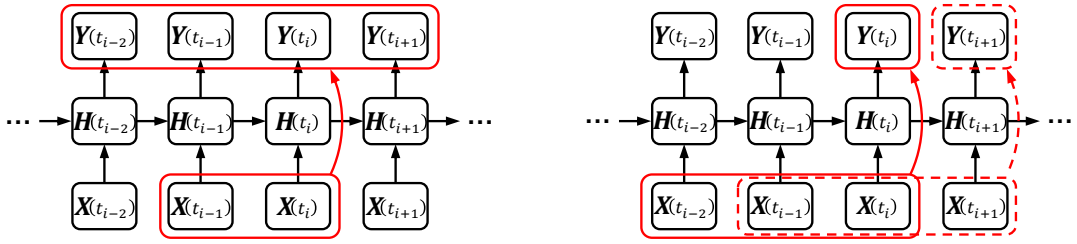

(a) $\boldsymbol{X}(t_{i-k}, \dots, t_i) \rightarrow \boldsymbol{Y}(t_j, \dots, t_{j+l})$ (b) $\boldsymbol{X}(t_{i-k}, \dots, t_i) \rightarrow \boldsymbol{Y}(t_i)$

Figure 4. Two structures to predict time-dependent processes using surrogate models without inherent time-dependent characteristics: (a) prediction of one output vector composed of various time instances using input features at multiple time instances, and (b) prediction of output at each time instance using input features at multiple time instances. Red rectangles indicate the inputs and outputs selected to form the input and output vectors.

4.2 Design of input vector

Two aspects are involved when designing the input vector: the selection of features included at each time instance (i.e., the specific form of $X(t_i)$ in Figure 4) and the time instances to stack these features (i.e., the selection of $(t_{i-k}, \dots, t_i)$ in Figure 4). The former affects all five models, and the latter affects only Models 1~4 (see Table 2), as the time-dependent structure of Model 5 does not require such stacking. Since the target output vector Y is simulated from a numerical model driven by wind and pressure fields, the seven hurricane parameters that define the wind and pressure fields and the water depth (sum of still water depth and tide level) are the most straightforward features to include in the input vector. Other features, including the maximum wind speed within the entire wind field, local wind speed at the selected site, and local wind direction, are also considered. The two circular variables, the hurricane translational direction and local wind direction, are expressed in terms of sinusoidal and cosinoidal values, as is common practice. As such, a total of 13 features are considered for each time instance.

For Models 1~4, the 13 input features are stacked at various time instances to form the input vector. Up to 9 time instances with 3-hour intervals are selected (i.e., t_i, $t_{i-3,}$…, t_{i-24}). For Model 1, only one training sample is extracted for each hurricane, and t_i is selected as the hour of the maximum V at the selected site, and the output time instances $(t_j, \dots, t_{j+l})$ include the 12 hours before and

after t_i (i.e., 25 time instances in total). The design of the input vector directly affects the effectiveness of the surrogate model, and much research has been devoted to optimizing the input vector [30, 31]. In preliminary experiments, fewer time instances and features at each time instance are tested, and the results indicate that using all 13 features at each time instance always yields the best prediction performance for Models 1~5. For Models 1, 3, and 4, stacking the 13 features at all 9 time instances yields the best prediction performance, while for Model 2, no stacking of the 13 features (i.e., using only the 13 features at t_i as the input vector) yields the best prediction performance.

4.3 Model training and evaluation

The five models considered in this paper use three types of surrogate models and three time-dependent structures, see Table 1 and Table 3. As such, the training and evaluation processes are slightly different for each model. For the 5,881 hurricanes included in the database of metocean conditions, 881 hurricanes are used for model evaluation (see Figure 5), leaving 5,000 hurricanes (~800,000 hurricane hours) for model training. The Kriging models are trained using the DACE package [20] in MATLAB, and the Neural Networks are trained using TensorFlow [32]. The training datasets are described for each prediction model as follows.

- For Model 1, all 5,000 hurricanes are used for training, producing 5,000 training samples.
- For Model 2, model training is based on hurricane hours rather than hurricanes, and therefore 5,000 hurricane hours are randomly selected from the 5,000 hurricanes as the training dataset. According to the result of the random selection, a total of ~3,000 hurricanes contribute to the 5,000 hurricane hours. The same number of 5,000 training samples is selected for Model 2 because (1) this allows a fair comparison with Model 1 to reveal the impact of the time-dependent structure on predictions and (2) it is intractable for the Kriging model to memorize ~800,000 training samples formed in terms of hurricane hours, as it takes ~5,000 Gigabytes of computer memory just to construct the $\boldsymbol{R}$ matrix in MATLAB using double-precision floating-point values for ~800,000 training samples.
- For Model 3, 5,000 training samples are used again to train the MLP model to create a fair comparison with the Kriging model in Model 2. Since there are more hyperparameters for Neural Networks than Kriging models, the chance of overfitting (i.e., the model learns not only the general trend but also the local, noise-like variations, resulting in testing performance that is much worse than the training performance) is higher. To prevent overfitting, a common approach is employed: a validation dataset is prepared in addition to the training dataset, and optimal hyperparameters are selected based on the performance of the model for the validation dataset, rather than for the training dataset. The ratio between the training dataset the validation dataset used here is around 70:15. As such, a total of 1,070 samples of hurricane hours are used for validation. The training and validation datasets are shuffled and re-divided during the training process to improve training efficiency.
- For Model 4, the ~800,000 hurricane hours are divided into ~660,000 samples for training and ~140,000 samples for validation according to the 70:15 ratio. The training process is the same as for Model 3.
- For Model 5, the training samples are formed in terms of hurricane hours, but the training process is done in terms of hurricanes, as time instances are fed into the model in sequence for each hurricane, see Section 2.3. As such, training and validation datasets are divided based on individual hurricanes.

The division of the 5,881 hurricanes in the catalog among training, validation, and testing datasets is illustrated in Figure 5. All models are tested for the same 881 hurricanes.

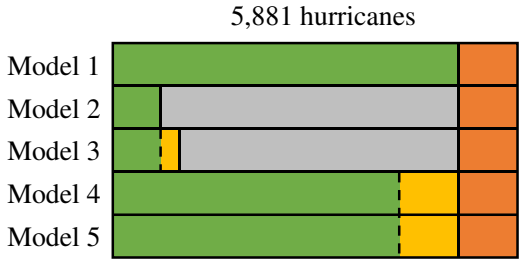

Figure 5. Division of the training (in green), validation (in yellow), and testing (in orange) datasets for each model.

5. Results and discussions

For the four types of metocean conditions (H_s, T_p, θ_{H_s}, and η), separate prediction models are trained and results of the H_s predictions are used as an example to compare the models. The overall performance of the models is presented in Section 5.1, and detailed comparisons are discussed in Section 5.2.

5.1 Overall performance

Models 1~5 are trained in different ways but are tested for the same 881 testing hurricanes. The root-mean-square error for the testing dataset is chosen as the metric to evaluate the performance of each model, expressed as,

$$\sigma_{Test} = \sqrt{\frac{1}{N}\sum_{i=1}^{m}\sum_{j=1}^{n_i}\left(\hat{y}_{i,j} - y_{i,j}\right)^2} \tag{7}$$

where $\hat{y}$ is the prediction value during a time instance of a hurricane, y is the corresponding true value from the numerical time-history simulation, subscript j indicates the prediction time instance, subscript i indicates the testing hurricane, m is the total number of testing hurricanes, which is 881 in this case, n_i is the total time instances for each testing hurricane, and N indicates the total time instances included in the testing hurricanes. Note that for the same hurricane, n_i is different for each prediction model. For instance, Model 1 provides predictions for 25 time instances regardless of the hurricane duration, while Models 2~4 provide predictions for a duration slightly shorter than the hurricane, since the mapping of $\boldsymbol{X}(t_{i-k}, \ldots, t_i) \rightarrow \boldsymbol{Y}(t_i)$ determines that the first available time instance for prediction is t_{k+1}; Model 5 provides predictions for the entire hurricane duration. As such, the number of time instances involved in σ_{Test} is different for each prediction model.

Each prediction model is tested for various sets of hyperparameters (see Table 1). The best performance for predicting H_s and the corresponding hyperparameters are listed in Table 4. Overall, Model 1 performs the worst, with $\sigma_{H_s,\mathrm{Test}} = 0.41$ m, and Model 5 performs the best, with $\sigma_{H_s,\mathrm{Test}} = 0.05$ m. The model performance is revealed with more details in Figure 6, which plots $\sigma_{H_s,\mathrm{Test}}$ versus H_s. It is interesting to note that $\sigma_{H_s,\mathrm{Test}}$ for Models 1 and 2 differs by ~32% as listed

in Table 4, while the H_s~$\sigma_{H_s,\mathrm{Test}}$ curves behave quite similar for H_s > 2 m. This is because the values of H_s predicted by Model 1 are all relatively high because of the way the hurricane duration is defined for Model 1, while the predictions of Model 2 cover almost the entire history of each hurricane. For the latter case, the majority of H_s values are low when the hurricane is far away, and the low values of $\sigma_{H_s,\mathrm{Test}}$ for H_s < 2 m lead to a lower value of $\sigma_{H_s,\mathrm{Test}}$. For risk analysis, which focuses on extreme conditions, a lower prediction error at high values of H_s is preferable compared to the trend in Figure 6, and this can be taken into account by including more intense hurricanes in the training database and by adjusting the training process to increase the weight of high values of H_s during the model training.

Table 4. The best prediction performance on the testing dataset and the corresponding network structure for the five models in Table 1.

	$\sigma_{H_s,\mathrm{Test}}$ (m)	Network structure
Model 1	0.41	-
Model 2	0.36	-
Model 3	0.19	3 × 1024
Model 4	0.14	5 × 32
Model 5	0.05	3 × 128

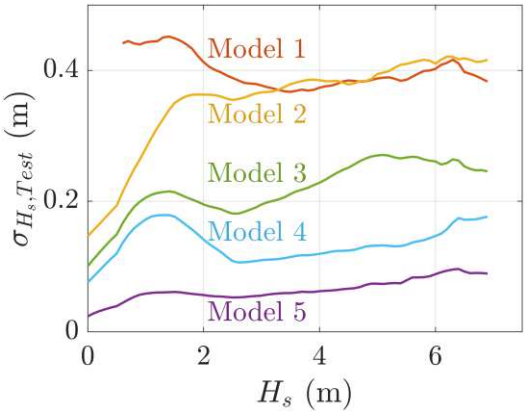

Figure 6. Prediction errors as a function of H_s.

Prediction performance of Model 5, which performs the best for H_s among the five prediction models, is provided in Table 5 for the other three metocean conditions (T_p, θ_{H_s}, and η). Note that for the prediction of θ_{H_s}, which is a circular variable, the output variable is selected as $\sin\theta_{H_s}$ and $\cos\theta_{H_s}$, so that values referring to the same direction (e.g., -180° and 180°) have the same representation. However, $\sigma_{T_p,\mathrm{Test}}$ is evaluated based on the resulting direction errors for the range between -180° and 180°.

To better illustrate the level of accuracy of Model 5 on various metocean conditions, prediction results for an individual hurricane that has a similar value σ_{Test} as the overall value provided in Table 4 are presented in Figure 7, with σ_{Test} for H_s, T_p, θ_{H_s}, and η equal to 0.04 m, 1.52 s, 13.5° , and 0.06 m, respectively. Note that the duration of the hurricane plotted in Figure 7 is 163 hours, but only the results for the 24 hours before and after the maximum H_s are shown here. The prediction of H_s matches the details of the simulation, while the prediction of T_p captures only the

overall trend of the simulation. Because θ_{H_s} is decomposed into sinusoidal and cosinoidal values during model training, the wrapping effect is captured (i.e., values higher than 180° reset to -180°) clearly. Note that Figure 7(c) shows a lower prediction error compared to the overall $\sigma_{\theta_{H_s}}$ of 13.5° . This is because of some large prediction errors when the hurricane is far away from the site of interest. An opposite situation is observed in Figure 7(d), where an overestimation at the peak surge is not reflected in the relatively low value of σ_η for this hurricane. These situations could be clarified with an alternative metric for performance, such as σ_{Test} for the time instances when the hurricane is close to the site of interest.

Table 5. The best prediction performance of Model 5 on the testing dataset and the corresponding network structures.

	Network structure	σ_{Test}
T_p	3×256	1.38 s
θ_{H_s}	5×512	15.4°
η	7×128	0.05 m

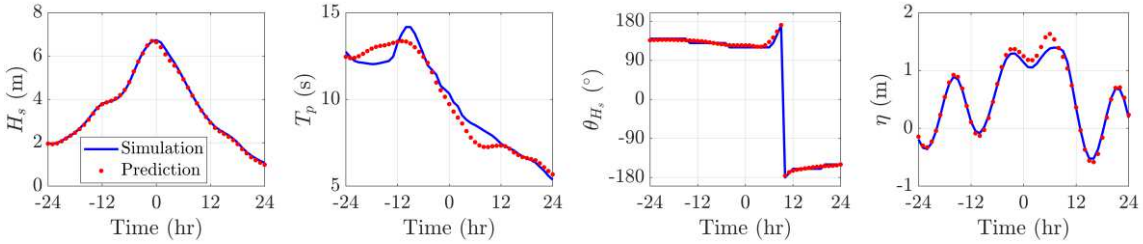

(a) *(b)* *(c)* *(d)*

Figure 7. Time history prediction of a) H_s, b) T_p, c) θ_{H_s}, and d) η for a testing hurricane. Hour zero is selected as the time of maximum H_s.

5.2 Detailed comparisons

Some key aspects of the five prediction models are summarized as follows to clarify the validity of comparisons among the models.

- Model 1 and Model 2 both use the Kriging model and are trained using 5,000 training samples. Model 1 is trained based on hurricanes (i.e., one training sample per hurricane), but Model 2 is trained based on hurricane hours (i.e., multiple training samples per hurricane).
- Model 2 and Model 3 use the same number of training samples and time-dependent structure. Model 2 uses the Kriging model, but Model 3 uses the MLP model, which is the most basic form of Neural Networks.
- Model 3 and Model 4 use the MLP model and the same time-dependent structure. Model 3 is trained using 5,000 training samples, while Model 4 is trained using ~660,000 training samples.
- Model 4 and Model 5 are trained using the same ~660,000 training samples. Model 4 uses the MLP model, which cannot inherently represent time-dependent behavior and relies on stacking input features at multiple time instances to represent such behavior. Model 5 uses the RNN-GRU model, which predicts the time-dependence of metocean conditions using its inherent recurrent structure.

5.2.1 Effect of time-dependent structure

The Kriging model is used to implement two structures of time-dependence as represented by Models 1 and 2, which can be expressed as $\boldsymbol{X}(t_{i-k}, \dots, t_i) \rightarrow \boldsymbol{Y}(t_j, \dots, t_{j+l})$ and $\boldsymbol{X}(t_{i-k}, \dots, t_i) \rightarrow \boldsymbol{Y}(t_i)$. As revealed in Figure 6, these two models perform similarly for H_s > 2 m. However, Model 2 outperforms Model 1 in two ways. First, Model 2 is more flexible in predicting hurricanes with varying duration, as Model 1 only provides predictions with a fixed duration. Second, Model 2 is more efficient in terms of how the simulated hurricanes are used for training. Even though the same number of training samples are used, Model 1 uses all 5,000 simulated hurricanes, while Model 2 uses only 5,000 hurricane hours (contributed by ~3,000 hurricanes), which is a small fraction of the ~800,000 total hurricane hours from the 5,000 hurricanes. The efficiency of these two strategies reflects the difference in what the models are learning from the training data. For Model 1, one set of input features related to the time instance of maximum local wind speed is used to predict the corresponding time history output, while for Model 2, each set of input features is used to predict the output at a corresponding time instance. As such, Model 1 learns how to represent metocean conditions during the *maximum* local wind input of a hurricane, while Model 2 learns to represent metocean conditions during *any* wind input of a hurricane.

5.2.2 Kriging vs. Neural Networks

The time-dependent structure $\boldsymbol{X}(t_{i-k}, \dots, t_i) \rightarrow \boldsymbol{Y}(t_i)$ is highly efficient, resulting in a large number of training samples, as the number of samples is approximately equal to the total hurricane hours instead of the number of hurricanes. Kriging models must memorize the entire training dataset, and thus the training process becomes intractable for large training datasets. There are some approaches (such as the adaptive Kriging combined with importance sampling method [33]) to improve efficiency in designing the training dataset, however, for a given training database, the comparison between Model 2 and Model 3 clearly shows how the type of surrogate model affects the prediction performance. The same number of 5,000 training samples are used in Model 2 and Model 3, and Model 3 using MLP lowers $\sigma_{H_s,\mathrm{Test}}$ by 32% compared to Model 2 using Kriging. The improvement is even more pronounced for high values of H_s, as shown in Figure 6. The MLP model outperforms Kriging because its capacity to approximate a nonlinear process can be easily adjusted through the network structure, while Kriging models provide limited hyperparameters (i.e., the selection of regression and correlation functions) to control its ability to approximate the nonlinear behavior of a process.

Another important difference between the Kriging models and the Neural Networks is that for the input included in the training dataset, Kriging models always provide an exact prediction for the corresponding training output, much like interpolation; while Neural Networks make predictions with some deviation from the corresponding training output, much like regression. For predictions of a spatial variable, where Kriging models are widely used, this characteristic is attractive because the input is well defined by the spatial coordinates. For hurricane metocean conditions, however, a regression-type behavior is more attractive, because the characteristics of a hurricane can rarely be well defined by several parameters at several time instances, i.e., the same hurricane input features can be used to describe different hurricanes, leading to variation in metocean conditions. Though there are ways to account for such variation in Kriging models [34], additional hyperparameters are required.

5.2.3 Size of the training dataset

One advantage of Neural Networks compared to Kriging models is that model training is no longer constrained by the size of the training dataset. Model 4 uses the same training process as Model 3, except that the entire ~660,000 training samples are used. The resulting overall value of $\sigma_{H_s,\mathrm{Test}}$ is reduced by 26%, and $\sigma_{H_s,\mathrm{Test}}$ is almost reduced by half for relatively high values of H_s (see Figure 6).

The training of Neural Networks effectively minimizes the training error. Due to the non-convex characteristics of the loss function, the mini-batch gradient descent algorithm is used as a standard approach in Deep Learning, which is also used in this paper. This algorithm uses a small number of training samples to estimate the gradient for minimizing the loss function and is more efficient and suitable when the size of the training data is large [35]. This also allows the model to be easily updated when new training samples are available, instead of re-training a model from scratch.

5.2.4 Neural Networks

Both Models 4 and 5 can be represented with the schematic in Figure 1. Model 4 uses a simple operation for each hidden layer as expressed in Eq. 2 and represents time-dependent processes by including hurricane features from previous time instances in the input layer. As such, the network learns the relationship between metocean conditions at each time instance and hurricane features at multiple time instances. Model 5 uses a much more complex operation for hidden layers as expressed in Eqs. 3~6 so that each hidden layer manages its own memory vector $\tilde{\boldsymbol{h}}_t$ representing the prediction history. The overall value of $\sigma_{H_s,\mathrm{Test}}$ for Model 5 is lowered by 64% compared to Model 4, and Figure 6 reveals that the values of $\sigma_{H_s,\mathrm{Test}}$ for Model 5 are about half of Model 4 for relatively high values of H_s. This suggests that using a network with an intrinsic time-dependent structure performs better than manually stacking input features. However, the better performance of Model 5 comes with a price. As shown in Figure 8, the performance of Model 5 is more sensitive to the network structure compared to Model 4. A U-shaped behavior is observed in Figure 8(b) for results based on networks with constant depth and varying width. The reason for this behavior is complex and is mainly due to the non-convex loss function within Neural Networks. Based on a study of the training and validation details, which is not presented here, some deep and narrow networks (e.g., a 5 × 16 network) converge to a local minimum of the loss function (i.e., a global minimum exists but is missed by the training algorithm) and thus perform worse compared to a shallower network with the same width. For a wide network (e.g., one with 4,096 units per hidden layer), when the number of hidden layers is large (starting from 3 hidden layers in this case), the training process becomes intractable due to the network complexity. For intermediate numbers of units per layer, a relatively clear pattern is observed: the prediction performance is insensitive to the number of hidden layers as long as more than one hidden layer is used, and the optimal number of units per layer is around 128. As such, it takes significantly more effort to test the network structure of the RNN-GRU model to reach its optimal performance compared to MLP.

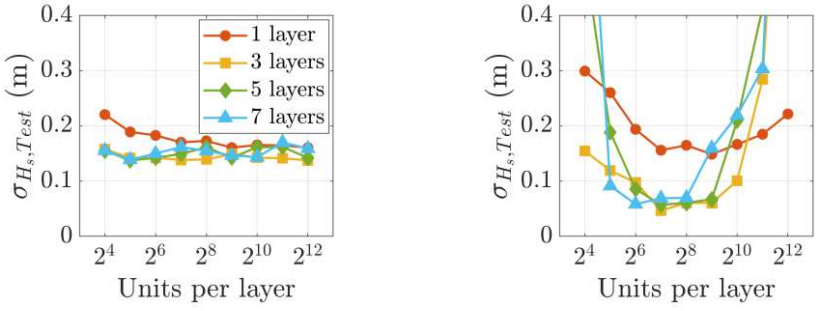

(a) *(b)*

Figure 8. The impact of the network width on model performance for a) Model 4 and b) Model 5.

6. Conclusions

Multiple approaches to apply surrogate models to predict time-dependent metocean conditions during hurricanes are discussed and implemented in this paper. A hurricane database composed of numerical metocean simulations for synthetic hurricanes is used for training and testing the surrogate models.

Some surrogate models, such as Kriging and Multilayer Perceptron, do not have the inherent ability to model time-dependent processes. However, by stacking inputs and/or outputs at various time instances, these models can be adapted to model time-dependent processes. Two adaptations are evaluated in this paper: $\boldsymbol{X}(t_{i-k}, \dots, t_i) \rightarrow \boldsymbol{Y}(t_j, \dots, t_{j+l})$ and $\boldsymbol{X}(t_{i-k}, \dots, t_i) \rightarrow \boldsymbol{Y}(t_i)$. The latter is found to utilize training data more efficiently as multiple training samples are produced by each hurricane. In addition, for these adapted models, larger sizes of the training dataset are found to improve prediction performance, but also increase computational demands, an issue that is especially pronounced for memory-based models such as Kriging.

Neural Networks are demonstrated to have great potential for time-dependent surrogate modeling for metocean conditions. They outperform the Kriging model in several respects. First, the RNN-GRU model illustrates extraordinary ability in predicting four metocean variables (significant wave height, peak wave period, peak wave direction, and sea surface elevation) during hurricanes (see Table 5 and Figure 7), an ability that can lower uncertainty when applying surrogate modeling in risk analysis and other tasks. Second, the complexity of Neural Networks can be adjusted easily through the network structure, which enables the models to learn the complex behavior of metocean conditions accurately. Lastly, the optimization algorithm for Neural Network can consider large training datasets efficiently, facilitating the processes of model training and updating. The flexibility of Neural Networks, however, makes their performance sensitive to the hyperparameters, and the complex RNN-GRU model implemented in this paper is shown to be especially sensitive.

The results of this paper strongly demonstrate the potential of Neural Networks and Deep Learning to represent complex metocean conditions during hurricanes, a potential that could transform the way hurricane risk is assessed.

Acknowledgment

The authors wish to thank Dr. Weichiang Pang for providing the synthetic hurricane catalog. This manuscript is based upon work supported by the National Science Foundation under Grant No. CMMI-1552559 and Northeastern University. Any opinions, findings, and conclusions expressed in this material are those of the authors and do not necessarily reflect the views of the National Science Foundation or other sponsors.

Reference

[1] I. R. Young, "Parametric Hurricane Wave Prediction Model," *J Waterw Port C-Asce,* vol. 114, no. 5, pp. 637-652, 1988. [Online]. Available: <Go to ISI>://WOS:A1988P956200006.

[2] H. L. Tolman, *User manual and system documentation of WAVEWATCH III v4.18*. 2014.

[3] DHI, *MIKE21 SW Scientific Documentary*. Denmark: DHI Water and Environment, 2014.

[4] J. Mahjoobi and A. Etemad-Shahidi, "An alternative approach for the prediction of significant wave heights based on classification and regression trees," *Appl Ocean Res,* vol. 30, no. 3, pp. 172-177, 2008.

[5] A. A. Taflanidis, G. Jia, A. B. Kennedy, and J. M. Smith, "Implementation/optimization of moving least squares response surfaces for approximation of hurricane/storm surge and wave responses," *Natural Hazards,* vol. 66, no. 2, pp. 955-983, 2012, doi: 10.1007/s11069-012-0520-y.

[6] G. F. Jia and A. A. Taflanidis, "Kriging metamodeling for approximation of high-dimensional wave and surge responses in real-time storm/hurricane risk assessment," (in English), *Computer Methods in Applied Mechanics and Engineering,* vol. 261, pp. 24-38, Jul 15 2013, doi: 10.1016/j.cma.2013.03.012.

[7] S. C. James, Y. Zhang, and F. O'Donncha, "A machine learning framework to forecast wave conditions," *Coast Eng,* vol. 137, pp. 1-10, 2018.

[8] G. F. Jia, A. A. Taflanidis, N. C. Nadal-Caraballo, J. A. Melby, A. B. Kennedy, and J. M. Smith, "Surrogate modeling for peak or time-dependent storm surge prediction over an extended coastal region using an existing database of synthetic storms," *Natural Hazards,* vol. 81, no. 2, pp. 909-938, Mar 2016, doi: 10.1007/s11069-015-2111-1.

[9] R. van der Merwe, T. K. Leen, Z. Lu, S. Frolov, and A. M. Baptista, "Fast neural network surrogates for very high dimensional physics-based models in computational oceanography," *Neural Netw,* vol. 20, no. 4, pp. 462-78, May 2007, doi: 10.1016/j.neunet.2007.04.023.

[10] S. Mandal and N. Prabaharan, "Ocean wave forecasting using recurrent neural networks," *Ocean Eng,* vol. 33, no. 10, pp. 1401-1410, 2006.

[11] W. W. Hsieh and B. Tang, "Applying neural network models to prediction and data analysis in meteorology and oceanography," *B Am Meteorol Soc,* vol. 79, no. 9, pp. 1855-1870, 1998.

[12] P. Jain and M. Deo, "Neural networks in ocean engineering," *Ships and offshore structures,* vol. 1, no. 1, pp. 25-35, 2006.

[13] A. Herman, "NEURAL-NETWORK MODELING AND DATA ANALYSIS TECHNIQUES IN COASTAL HYDRODYNAMIC STUDIES—A REVIEW," L. L. Wright Ed.: Nova Science Publishers, 2011.

[14] S.-W. Kim, J. A. Melby, N. C. Nadal-Caraballo, and J. Ratcliff, "A time-dependent surrogate model for storm surge prediction based on an artificial neural network using high-fidelity synthetic hurricane modeling," *Natural Hazards,* vol. 76, no. 1, pp. 565-585, 2014, doi: 10.1007/s11069-014-1508-6.

[15] A. Herman, R. Kaiser, and H. D. Niemeyer, "Wind-wave variability in a shallow tidal sea—Spectral modelling combined with neural network methods," *Coast Eng,* vol. 56, no. 7, pp. 759-772, 2009.

[16] M. Browne, B. Castelle, D. Strauss, R. Tomlinson, M. Blumenstein, and C. Lane, "Near-shore swell estimation from a global wind-wave model: Spectral process, linear, and artificial neural network models," *Coast Eng,* vol. 54, no. 5, pp. 445-460, 2007.

[17] R. Collobert and J. Weston, "A unified architecture for natural language processing: Deep neural networks with multitask learning," in *Proceedings of the 25th international conference on Machine learning*, 2008: ACM, pp. 160-167.

[18] C. Szegedy, V. Vanhoucke, S. Ioffe, J. Shlens, and Z. Wojna, "Rethinking the inception architecture for computer vision," in *Proceedings of the IEEE conference on computer vision and pattern recognition*, 2016, pp. 2818-2826.

[19] K. Cho *et al.*, "Learning phrase representations using RNN encoder-decoder for statistical machine translation," *arXiv preprint arXiv:1406.1078,* 2014.
[20] S. Lophaven, H. Nielsen, and J. Sondergaard, "DACE: A Matlab Kriging Toolbox.," *Technical University of Denmark,* 2002.
[21] V. Nair and G. E. Hinton, "Rectified linear units improve restricted boltzmann machines," in *Proceedings of the 27th international conference on machine learning (ICML-10)*, 2010, pp. 807-814.
[22] D. P. Kingma and J. Ba, "Adam: A method for stochastic optimization," *arXiv preprint arXiv:1412.6980,* 2014.
[23] D.-A. Clevert, T. Unterthiner, and S. Hochreiter, "Fast and accurate deep network learning by exponential linear units (elus)," *arXiv preprint arXiv:1511.07289,* 2015.
[24] T. Tieleman and G. Hinton, "Lecture 6.5-rmsprop, coursera: Neural networks for machine learning," *University of Toronto, Technical Report,* 2012.
[25] F. Liu, "Projections of Future US Design Wind Speeds Due to Climate Change for Estimating Hurricane Losses," Clemson University, 2014.
[26] P. N. Georgiou, A. G. Davenport, and B. J. Vickery, "Design Wind Speeds in Regions Dominated by Tropical Cyclones," (in English), *J Wind Eng Ind Aerod,* vol. 13, no. 1-3, pp. 139-152, 1983, doi: Doi 10.1016/0167-6105(83)90136-8.
[27] G. J. Holland, "An Analytic Model of the Wind and Pressure Profiles in Hurricanes," (in English), *Mon Weather Rev,* vol. 108, no. 8, pp. 1212-1218, 1980, doi: 10.1175/1520-0493(1980)108<1212:aamotw>2.0.co;2.
[28] C. Qiao, A. Myers, and S. R. Arwade, "Validation of a 37-year Metocean Hindcast along the U.S. Atlantic Coast," presented at the 13th International Conference on Applications of Statistics and Probability in Civil Engineering, ICASP13, Seoul, South Korea, May, 2019.
[29] DHI, *MIKE21-FM HD Scientific Documentary*. Denmark: DHI Water and Environment, 2014.
[30] K. Kira and L. A. Rendell, "A practical approach to feature selection," in *Machine Learning Proceedings 1992*: Elsevier, 1992, pp. 249-256.
[31] A. L. Blum and P. Langley, "Selection of relevant features and examples in machine learning," *Artificial intelligence,* vol. 97, no. 1-2, pp. 245-271, 1997.
[32] M. Abadi *et al.*, "Tensorflow: A system for large-scale machine learning," in *12th {USENIX} Symposium on Operating Systems Design and Implementation ({OSDI} 16)*, 2016, pp. 265-283.
[33] W. Yun, Z. Lu, X. J. S. Jiang, and M. Optimization, "An efficient reliability analysis method combining adaptive Kriging and modified importance sampling for small failure probability," vol. 58, no. 4, pp. 1383-1393, 2018.
[34] R. B. Gramacy, *Surrogates: Gaussian Process Modeling, Design, and Optimization for the Applied Sciences*. CRC Press, 2020.
[35] M. Li, T. Zhang, Y. Chen, and A. J. Smola, "Efficient mini-batch training for stochastic optimization," in *Proceedings of the 20th ACM SIGKDD international conference on Knowledge discovery and data mining*, 2014: ACM, pp. 661-670.

Figures

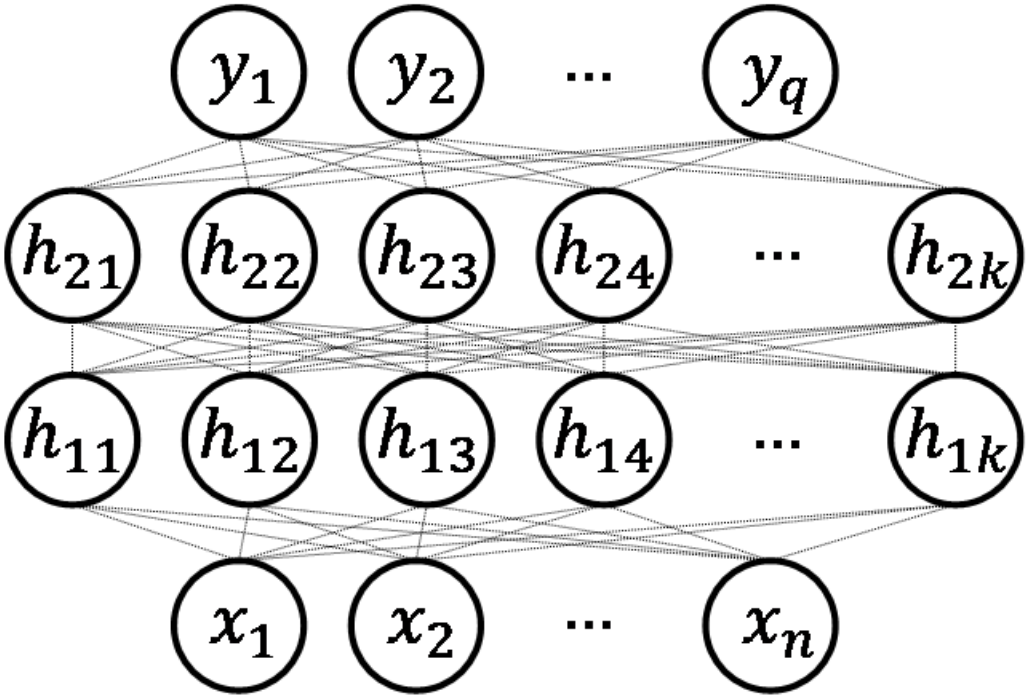

Figure 1

An example MLP model structure with l = 2 hidden layers and k units per hidden layer.

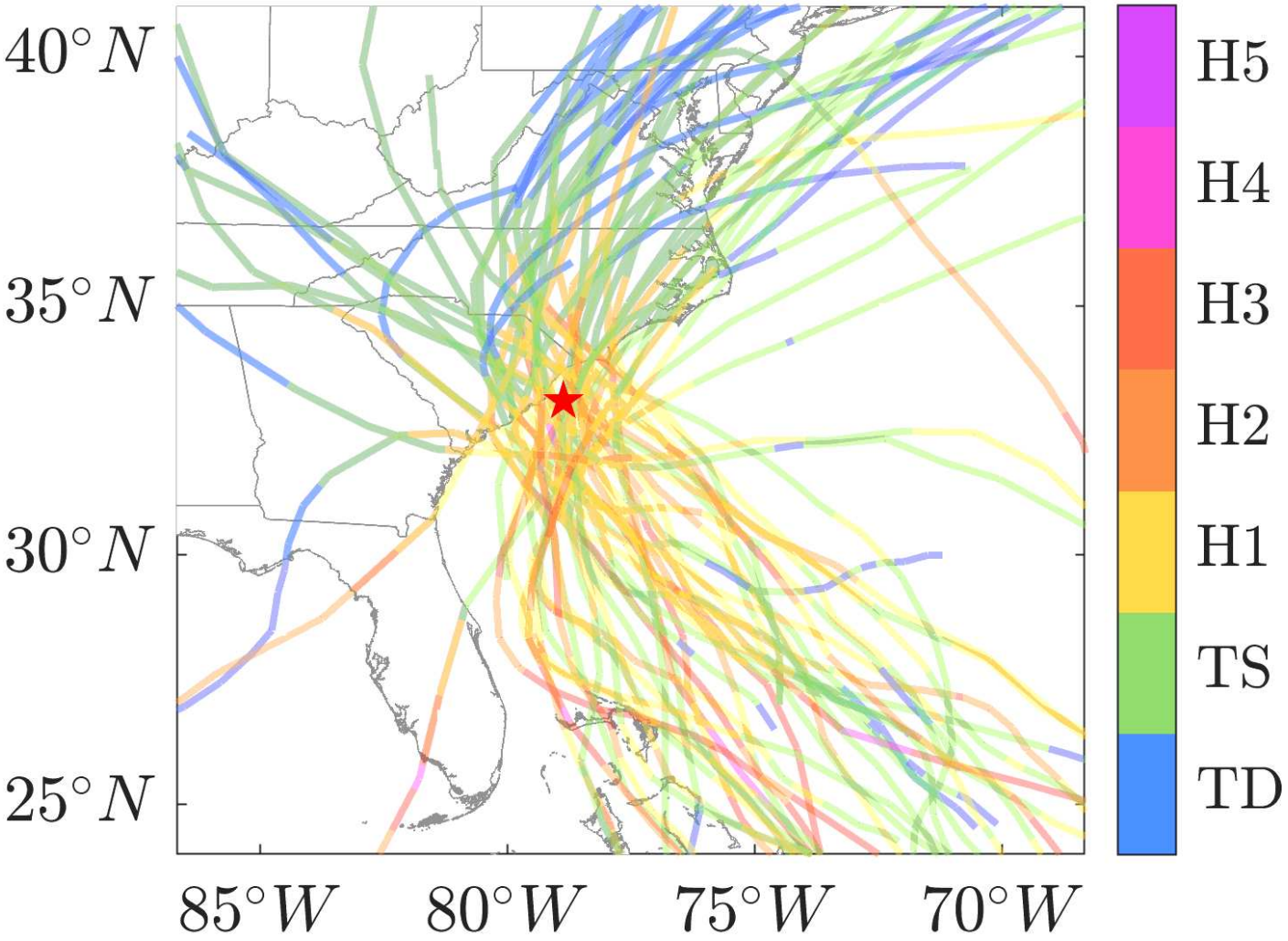

Figure 2

The location of the offshore site near South Carolina (red star) and the trajectories of 50 hurricanes randomly sampled from a total of 5,881 synthetic hurricanes included in the hurricane database. The color of the trajectory indicates the hurricane intensity per the Saffir-Simpson scale (TD stands for tropical depression and TS stands for tropical storm).

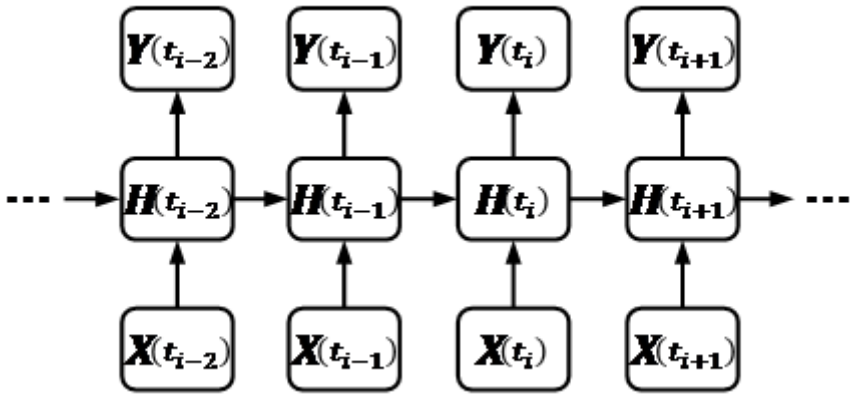

Figure 3

Schematic of the time-dependent structure of a sequence-to-sequence model, where subscripts indicate the time instance, X represents the input vector, H represents a vector of hidden variables, and Y represents the output vector

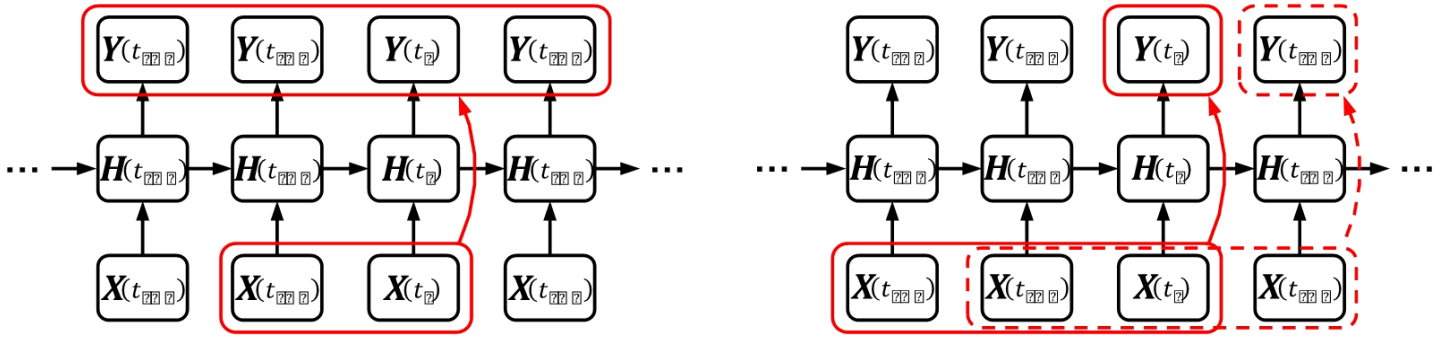

Figure 4

Two structures to predict time-dependent processes using surrogate models without inherent time-dependent characteristics: (a) prediction of one output vector composed of various time instances using input features at multiple time instances, and (b) prediction of output at each time instance using input features at multiple time instances. Red rectangles indicate the inputs and outputs selected to form the input and output vectors.

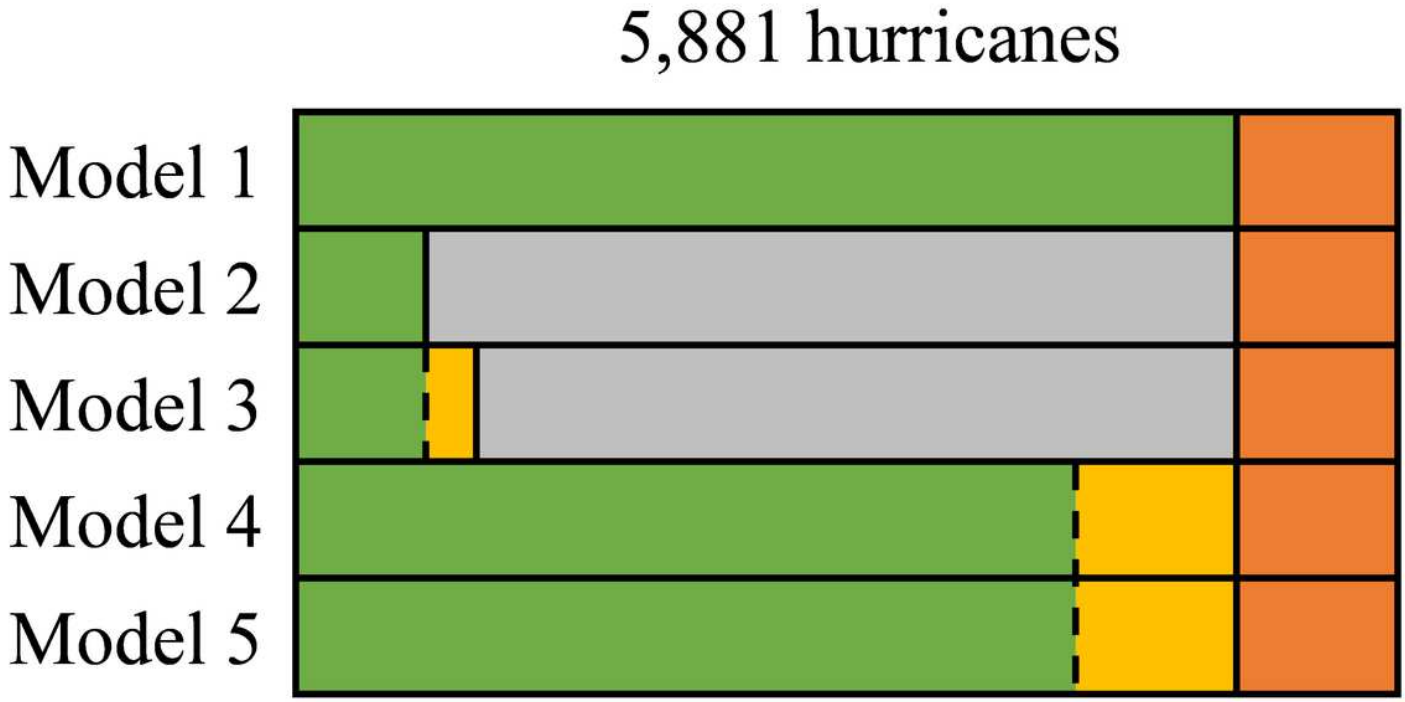

Figure 5

Division of the training (in green), validation (in yellow), and testing (in orange) datasets for each model.

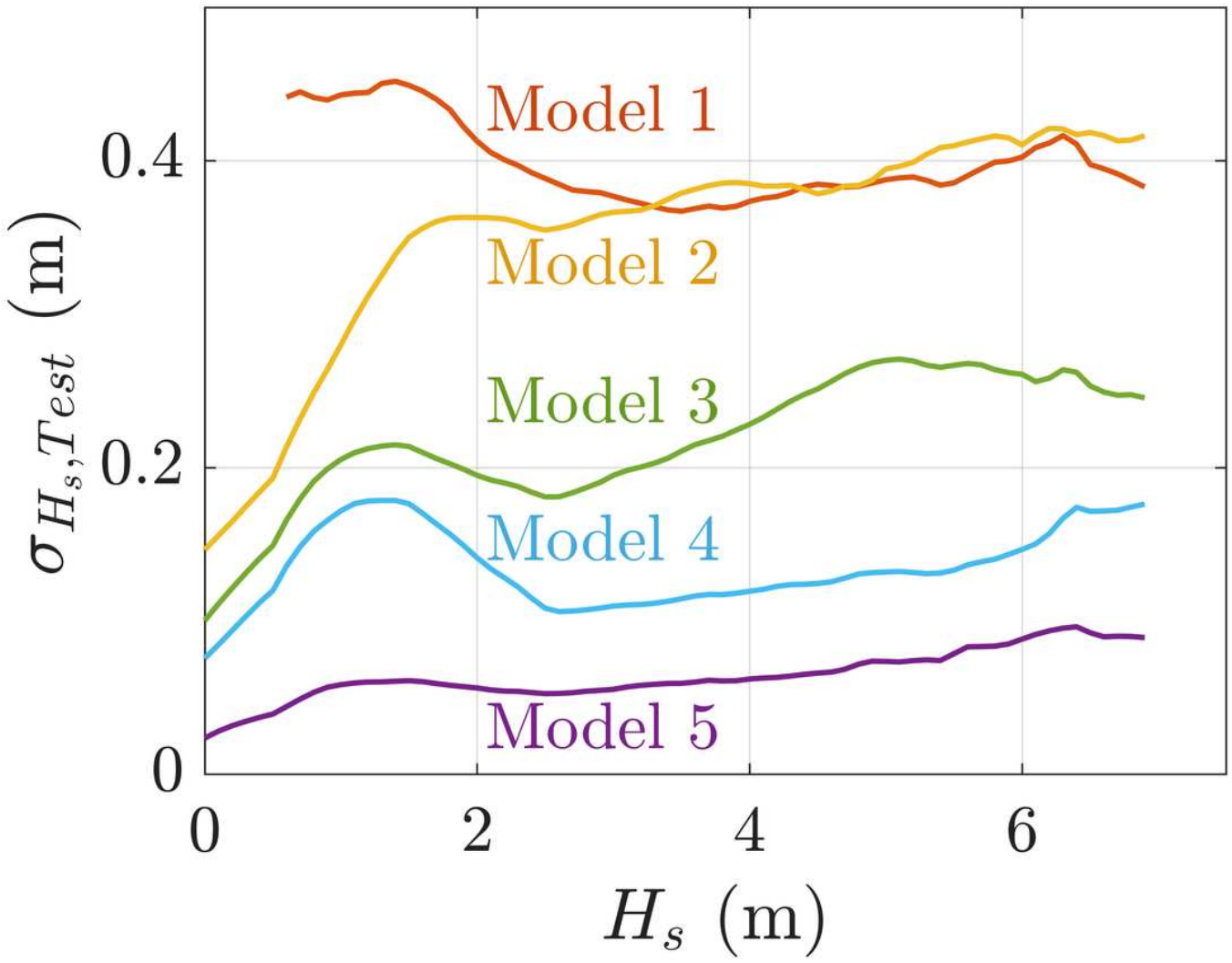

Figure 6

Prediction errors as a function of Hs.

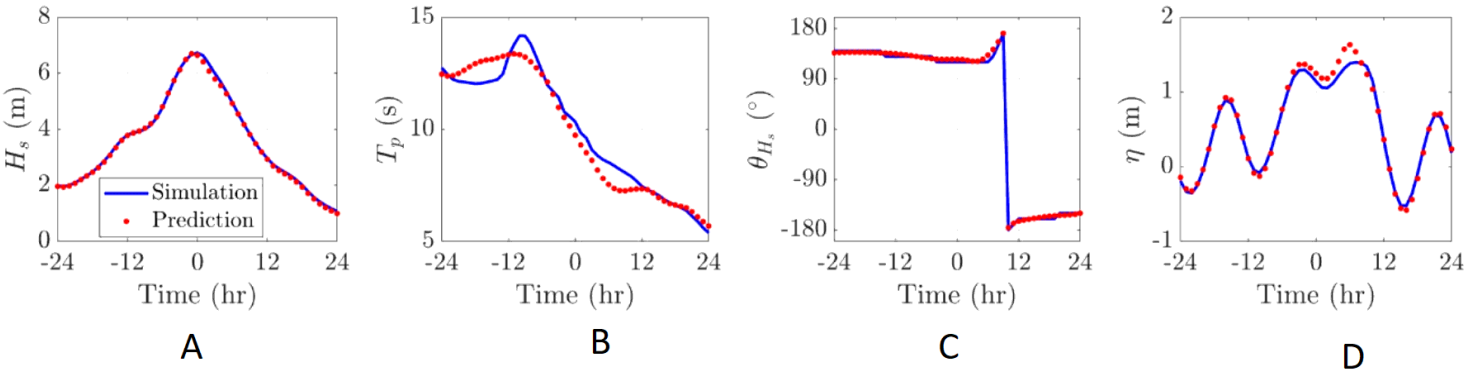

Figure 7

Time history prediction of a) Hs, b) Tp, c) θ(Hs), and d) η for a testing hurricane. Hour zero is selected as the time of maximum Hs.

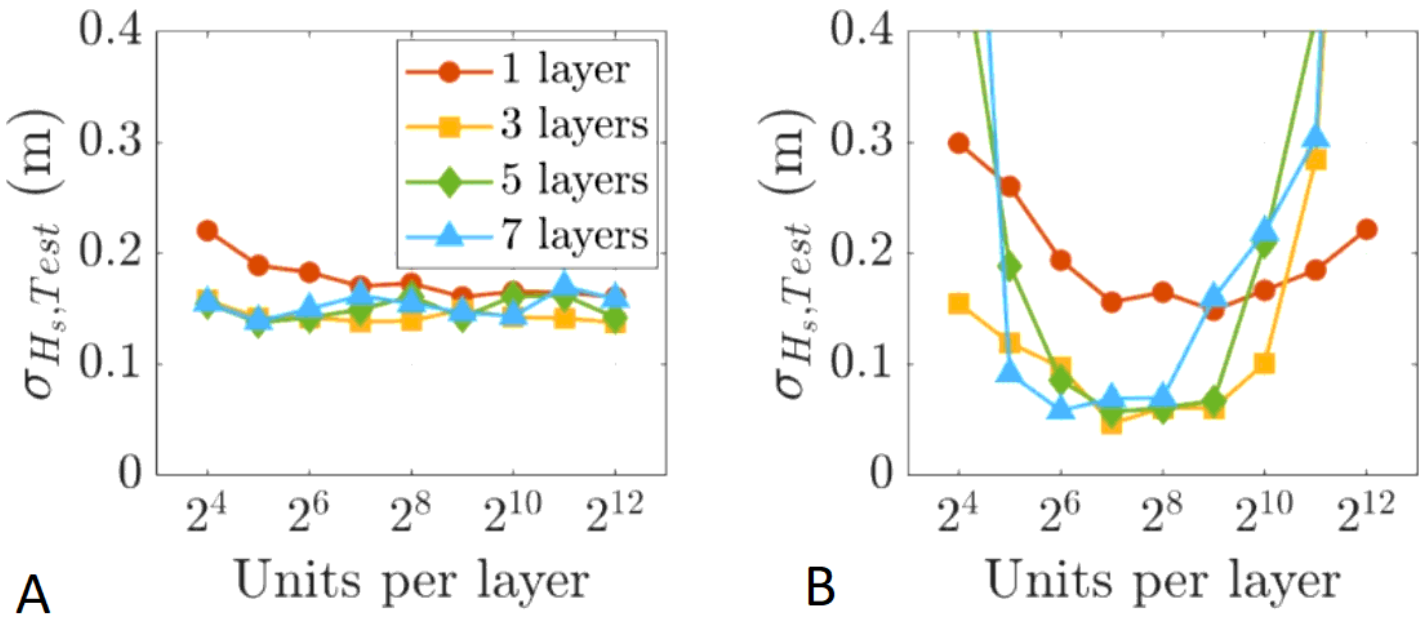

Figure 8

The impact of the network width on model performance for a) Model 4 and b) Model 5.